A Heuristic Description of Internal Wave Dynamics

KURT POLZIN

Department of Physical Oceanography, Woods Hole Oceanographic Institution, Woods Hole, Massachusetts

(Manuscript received 3 July 2003, in final form 24 July 2003)

ABSTRACT

The oceanic internal wave spectrum has long been interpreted as being shaped by nonlinear processes. The empirical Garrett and Munk synthesis of oceanic observations is $E(m, \omega) \propto Nm^{-2}\omega^{-2}$ at high wavenumber and frequency. Results of both approximate analytic and numerical estimates of weak nonlinear interactions under the resonant interaction approximation have previously been interpreted as implying the dominance of scale-separated interactions and that the Garrett and Munk spectrum is stationary with respect to the nonlinear interactions. However, dimensional analysis cobbled together with several basic observational constraints requires a stationary spectrum of $E(m, \omega) \propto Nm^{-2}\omega^{-3/2}$ at high vertical wavenumber and frequency. Given this stationary spectrum, dimensional analysis and extant data are used to infer a flux representation for the spectral transports. The resulting semiempirical flux laws can be described as a relaxation to the stationary power laws. The stationary spectrum is consistent with energy sources at low frequencies and dissipation at higher frequencies and vertical wavenumber. The analysis is then extended to include vertically asymmetric wave fields. Vertical wavenumber spectra of horizontal velocity that exhibit a difference between rotary (clockwise and counterclockwise phase rotation of the velocity vector with depth) spectra at large wavelengths tend to be symmetric at smaller scales. This pattern is hypothesized to be a result of nonlinearity within the wave field. In particular, vertical symmetry is linked here to the issue of momentum conservation. A backscattering process is invoked to achieve momentum conservation. This representation of nonlinearity is used in a numerical scheme to assess the spatial evolution of a bottom-generated wave field. The predicted patterns of relaxation and vertical symmetry are in reasonable agreement with finescale observations above rough bathymetry in the Brazil Basin.

1. Introduction

The oceanic internal wave literature is a disordered mélange. Research into the processes responsible for the observed wave field has numerous facets: generation by many plausible yet distinct mechanisms, linear propagation at turning points, interactions with geostrophic currents, nonlinear interactions between internal waves, reflection from planar sloping boundaries, scattering from irregular boundaries, and, finally, dissipation by instability and wave breaking. There are many fine reviews that create an ordered perspective of these pieces (e.g., Garrett and Munk 1975, 1979; Thorpe 1975; Munk 1981; Müller et al. 1986; Gregg 1987). In addition, the series of *'Aha Huliko'a* meeting reports is a rich source of material, distilled and otherwise. But there is an intrinsic disorder in that the various elements are usually not connected to each other in a systematic way. The most intrinsically difficult piece of a synthetic treatment is to account for nonlinearity and dissipation in the wave field. The key to a synthetic treatment is developing a sufficiently simple understanding of nonlinearity and wave breaking such that their effects can be more easily recognized and appreciated.

The tools for developing a simple understanding of nonlinearity and wave breaking are limited. Numerical simulations in the spatial/temporal domains are usually idealized, computationally intensive, resolve a limited range of scales, have issues with boundary conditions, and invoke subgrid-scale closures whose effects may not be fully appreciated. Alternately, one can consider solutions to a ''radiation balance equation'' (e.g., Müller and Olbers 1975), which describes the wave field in the spatial/temporal/spectral domains. Closures for the radiation balance equation are expressed in the spectral domain. The promise of this approach is the possibility of more easily separating the influences of forcing, propagation, boundary conditions, and nonlinearity. One drawback is the possible complexity of the closure. A second drawback is that no extant closure scheme is formally valid for internal waves having vertical wavelengths smaller than about 60 m.

The present work is primarily a tool-building exercise to construct a relatively simple closure for the internal wave radiation balance equation. The approach taken here is heuristic; a set of semiempirical flux laws is proposed. The intent is to use these flux laws to quantify patterns within the oceanic internal wave field and it-

Corresponding author address: Dr. Kurt Polzin, Department of Physical Oceanography, Woods Hole Oceanographic Institution, MS #21, Woods Hole, MA 02543.
E-mail: kpolzin@whoi.edu

eratively refine our knowledge of internal wave dynamics. The first product of this iterative approach examines the near-boundary decay of the finescale internal wave field and models of internal wave generation (Polzin 2004). A second effort (Lvov 2003, manuscript submitted to *Phys. Rev. Lett.*) reviews extant datasets and interprets variability of observed vertical wavenumber–frequency power laws in terms of a family of stationary states resulting from nonlinear interactions.

Implicit in this study is the notion that ''far'' from forcing regions and boundaries in the spectral/spatial/temporal domains, the internal wave field manifests the character of the underlying nonlinearity. In the far field, the spectrum will relax back to a characteristic shape that is stationary with respect to the nonlinearity. To be explicit, a stationary spectrum has the property that variance executes a nondivergent cascade through the spectrum. This cascade can be quantified at centimeter scales by identifying the spectral transport with the rate of dissipation of turbulent kinetic energy ϵ.

Several nonlinear interaction models exist (Müller et al. 1986). The first of these is based upon the fact that energy and momentum can be systematically transferred between internal wave triads if certain resonance criteria are met. This approach is generically referred to here as the resonant interaction approximation (RIA). The second considers the refraction of internal waves by the time-varying velocity field of other internal waves using eikonal (ray tracing) techniques. The results of the models are in general agreement but differ in details. Dissipation in both models is quadratically dependent upon spectral level and buoyancy frequency, and the energy transfers increase with increasing wave frequency. Differences include the power laws of the associated stationary spectra and the sign of the transport in the frequency domain. Neither model is formally valid when applied to the finescale oceanic internal wave field. Dimensional analysis is invoked here and, with the aid of observational studies, a detailed spectral transport scheme is developed that is independent of either model.

In section 2a, validation studies of existing wave–wave interaction models are critically examined. The intent is twofold: to summarize measurements relating turbulent dissipation to variability of the internal wave field and to dispel an apparent myth that resonant interaction schemes tend to overestimate observed transports. The radiation balance equation of Müller and Olbers (1975) is then modified in section 2b to describe the temporal evolution of spatially inhomogeneous internal wave spectra before developing a consistent representation of nonlinearity. This representation is based upon dimensional considerations and assumes that nonlinearity is unrelated to boundaries in the spectral domain. Nonlinearity is treated by first defining a stationary spectrum (section 2c) and then defining flux representations of spectral transports (section 2d). These flux representations have the character of relaxation back to the stationary spectrum. Section 3a briefly describes extant observations that relate to the issue of momentum conservation. Section 3b discusses the issue of momentum conservation in the context of a flux transport scheme for vertically asymmetric wave fields. The resulting momentum closure (section 3c) can be characterized as a backscattering process. This scheme is then used to briefly assess the spatial evolution of a bottom-generated wave field (section 4). The general patterns of spectral relaxation and variable asymmetry associated with backscattering are in reasonable agreement with finescale observations from the Brazil Basin. Last, a critical eye is turned to extant theories of nonlinear wave–wave interactions (section 5) with the intent of comparing those previous numerical and analytic results with the flux representations derived here.

2. Energy transports in the spectral domain

a. Observational constraints on transport schemes

Like waves on the ocean's surface, in which whitecapping and dissipation are related to the transport of energy to smaller scales as the net product of nonlinear interactions, turbulent dissipation in the stratified ocean interior can be interpreted as the product of nonlinear interactions between internal waves. The association is most tangible as the scale separation between waves and turbulence is reduced. Several different groups in the last 10–15 years have reported model validation studies relating the rate of dissipation of turbulent kinetic energy, ϵ, measured at centimeter scales, to variability in the finescale internal wave field over vertical wavelengths of tens to hundreds of meters.

The pioneering work of Gregg (1989) produced an observationally based estimate of turbulent dissipation (ϵ) associated with the Garrett and Munk spectrum:

$$\epsilon_{\rm obs} = 7 \times 10^{-10} \frac{N^2}{N_o^2} \frac{\langle S_{10}^4 \rangle}{\langle S_{10\rm GM}^4 \rangle} \ (\rm W\ kg^{-1}), \qquad (1)$$

with buoyancy frequency $N(z)$, a reference value N_o of (3 cph), and 10-m, first-difference shear estimates (S_{10}) referenced to the GM76 value, $S_{10\rm GM}$. Note that the Garrett and Munk spectrum refers to a series of empirical fits to oceanic spectra that attempt to characterize the background internal wave field. GM76 refers to the Garrett and Munk (1975) model as revised by Cairns and Williams (1976). M81 refers to the Munk (1981) revision. Gregg (1989) compared estimates of $\epsilon_{\rm obs}$ with two theoretical estimates of the energy flux through the internal wave spectrum to dissipation scales that were based on different representations of wave–wave interactions. The first of these, an approximate representation of the transport under the resonant interaction approximation (RIA; McComas and Müller 1981b), was reported to be an overestimate:

$$\epsilon_{\rm MM}^{\rm G89} \cong 3.4 \times \epsilon_{\rm obs}. \qquad (2)$$

The second model, based on eikonal (ray tracing) tech-

niques (HWF; Henyey et al. 1986), was deemed an underestimate:

$$\epsilon_{\mathrm{HWF}}^{\mathrm{G89}} \cong \epsilon_{\mathrm{obs}}/2. \tag{3}$$

Gregg (1989) made three mistakes in extracting results from McComas and Müller (1981b) and Henyey et al. (1986). The first two are discussed in Polzin et al. (1995): (i) Henyey et al. (1986) used the M81 version of the GM spectrum, and so, noting that $\langle S_{10\mathrm{M81}}^4 \rangle = \langle S_{10\mathrm{GM76}}^4 \rangle/2$, Gregg's data actually support

$$\epsilon_{\mathrm{obs}} \cong \epsilon_{\mathrm{HWF}}, \tag{4}$$

and (ii) Gregg (1989), when estimating $\epsilon_{\mathrm{MM}}^{\mathrm{G89}}$ as the sum of the fluxes associated with the parametric subharmonic instability (psi) and induced diffusion (id) mechanisms, incorrectly quoted the id transport as the quotient of the internal wave energy density and a time scale. The id transport is actually set by the psi transport and is about 40% of the total (Müller et al. 1986). (iii) The third error is that McComas and Müller (1981b) used a modified version of the GM spectrum, one without an inertial peak having a vertical wavenumber energy density $2/\pi$ times as small as the GM76 spectrum. Accounting for both errors in interpreting McComas and Müller (1981b), one obtains

$$\epsilon_{\mathrm{obs}} \cong \epsilon_{\mathrm{MM}}. \tag{5}$$

Thus, one cannot distinguish ϵ_{obs} from either ϵ_{MM} or ϵ_{HWF}: Both theoretical predictions agree with the data to within 20%. Note further that the two theoretical models share a functional similarity in the dependence of ϵ upon N and spectral level, as in (1).

Gargett (1990) further criticized Gregg (1989) for the following: (i) insufficient N variability within the observations to distinguish a scaling of N^2 from $N^{3/2}$ and (ii) S_{10} can be a biased estimate of the shear spectral level.

Wijesekera et al. (1993) tested modified versions of the above predictions for ϵ with data obtained from a wave field that contained significant high vertical wavenumber, high-frequency energy. The parameterizations used by Wijesekera et al. (1993) did not account for variations in the frequency content of the wave field and thus did not do a good job predicting the observed dissipation.

Polzin et al. (1995) tested data with sufficient range in N to address the issue of buoyancy scaling, appropriately analyzed the data in the spectral domain, and attempted to account for variability in ϵ associated with variability in the frequency content of the internal wave field. In particular, they tested a slight revision (Henyey 1991) of the Henyey et al. (1986) parameterization,

$$\epsilon_{\mathrm{HWF}} = 0.1 m_c N^{-1} \int_0^{m_c} m^2 E_k(m)\, dm \times \int_f^N \left(\frac{\omega^2 - f^2}{N^2 - \omega^2}\right)^{1/2} E(m_c, \omega)\, d\omega, \tag{6}$$

in which $E(m, \omega)$ is the vertical wavenumber–frequency $(m - \omega)$ energy density and integration over the frequency domain in (6) defines an energy-density-weighted aspect ratio, $k_h/m = [(\omega^2 - f^2)/(N^2 - \omega^2)]^{1/2}$ with Coriolis frequency f and wave vector $\mathbf{k} = (k, l, m)$ having horizontal magnitude $k_h = (k^2 + l^2)^{1/2}$. The vertical wavenumber spectrum $E_k(m)$ represents kinetic energy density; $E_p(m)$ represents potential energy. Integration of $E(m, \omega)$ over frequency is indicated by the presence of a single variable in the argument of E: $E(m) = \int_f^N E(m, \omega)\, d\omega$. A spectral cutoff at m_c is defined by

$$2 \int_0^{m_c} m'^2 E_k(m')\, dm' = 0.7 N^2. \tag{7}$$

With aspect ratios estimated from shear $[m^2 E_k(m)]$ and strain $[m^2 E_p(m)]$ spectra, (6) predicts the observed ϵ to within a factor of ± 2, the approximate statistical uncertainty of the measurements presented in Polzin et al. (1995) (Fig. 1). Aside from differences associated with the spectrum utilized by McComas and Müller (1981b), Polzin et al. (1995) report that variability in their data is insufficient to distinguish between the two model predictions.

Polzin et al.'s (1995) study encompassed observations that deviated from the GM spectral model [spectral amplitude, spectral shape in both the vertical wavenumber and frequency domain, asymmetry/anisotropy (nonequal distribution of spatial energy flux with respect to direction), and inhomogeneity (spatial gradients in N-scaled spectral amplitude)]. In order of decreasing importance, the dissipation rate was determined to depend upon N^2, the spectral amplitude, and the average frequency content of the internal wave field. Notably, the dissipation rate appeared to be insensitive to variations in the shape of the finescale vertical wavenumber spectrum, asymmetry, and inhomogeneity.

Carter and Gregg (2002) infer very poor agreement between these model predictions and observations from Monterey Canyon. Implicit in the comparison of ϵ with the model predictions is an assumption that energy cascades through the wavenumber domain. In Monterey Canyon, there is a spatial convergence of energy associated with the onshore propagation of nearly critical internal waves. These waves will undergo a transformation of spatial scales under reflection, and this transformation may well short circuit the normal cascade process. Indeed, since Kunze et al. (2002) find that $2\pi/m_c$ is larger than the total water column depth for their more energetic profiles, the data may not be sufficiently far from forcing and boundaries to invoke a cascade representation.

Implicit in (6) (and in the RIA) is an f scaling, that is, $\epsilon \propto |f|$, where f is the Coriolis parameter, for the background internal wave field. Data discussed by Gregg et al. (2003) document general agreement be-

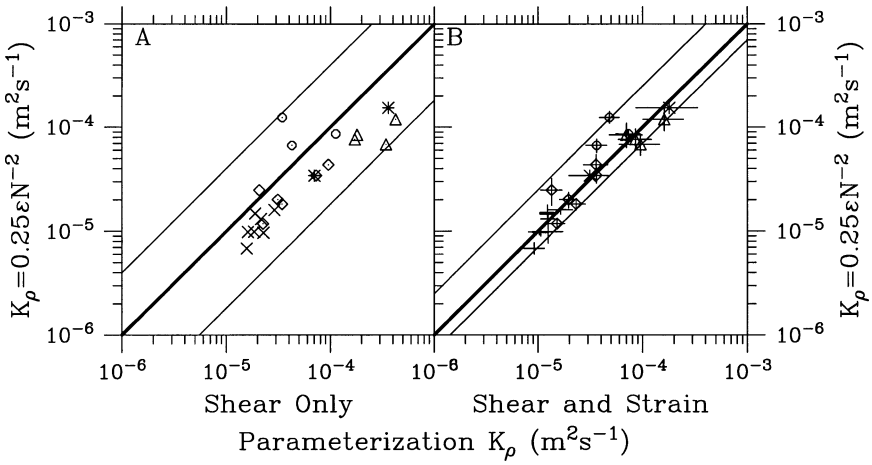

FIG. 1. Results of a model validation study from Polzin et al. (1995). The vertical axis represents observed centimeter-scale shear variance represented as diapycnal diffusivity ($K_\rho \propto \epsilon/N^2$); the horizontal axis represents (6) similarly presented as K_ρ. (a) A comparison between data and model without accounting for the frequency-dependent terms; (b) such terms are included. The thick diagonal line denotes agreement with (6). The various symbols represent different datasets. See Polzin et al. (1995) for further details.

tween (6) and observations obtained from mid- and low latitudes: ϵ decreases as $|f|$ decreases.

Given the functional similarity of the two dissipation predictions, and with $\epsilon_{\rm obs} \cong \epsilon_{\rm MM} \cong \epsilon_{\rm HWF}$, there is no observational support for one dynamical model over the other. What can be concluded, however, is that observed dissipation rates associated with wave–wave interactions depend quadratically upon N and energy density, and transports increase with increasing wave frequency. These observational constraints will be used to help construct flux representations in section 2c.

b. The radiation balance equation

In a wave packet derivation, for example, Phillips (1977), the evolution of a wave packet's amplitude is governed by a wave action conservation statement, which has an equivalent spectral representation as the radiation balance equation (cf. Müller and Olbers 1975):

$$\partial_t A(\mathbf{k}) + \nabla \cdot \mathbf{C}_g A(\mathbf{k}) + \nabla_{\mathbf{k}} \cdot \mathbf{F}(\mathbf{k}) = S_o(\mathbf{k}) - S_i(\mathbf{k}). \quad (8)$$

Here $A(\mathbf{k})$ is the action spectrum; $\mathbf{k}$ is a 3D wave vector; transports of $A(\mathbf{k})$ through the spectral domain are represented as $\mathbf{F}(\mathbf{k})$, sources by $S_o(\mathbf{k})$, and sinks as $S_i(\mathbf{k})$. There are several immediate problems associated with using (8) as the basis for a descriptive tool. The most daunting is that action is neither directly observed nor intrinsically conserved by internal wave–wave interactions. Internal wave interactions conserve energy and momentum, not action (Müller et al. 1986). See section 5 for further discussion.

The first step in the tool-building exercise is to construct a transport scheme that directly addresses the information content of the observations. This focus dictates the following: 1) Observations typically do not permit characterization of the field in terms of discrete wave packets, so a spectral representation is pursued. Conservation statements are constructed here using a simple kinematic box in the spatial/temporal/spectral domain. 2) Observations are generally obtained in the temporal and/or vertical spatial domain, rather than the horizontal, so that a description in terms of the vertical wavenumber and frequency domain is pursued rather than a 3D wave vector space. 3) Energy and momentum conservation are pursued here because wave energy and ϵ are the observed variables.

Consider a point (m_2, ω_2, z_2) in vertical wavenumber (m), frequency (ω), and vertical coordinate (z) space (Fig. 2). The energy density in the volume defined by the line segments $\Delta m = m_3 - m_1$, $\Delta\omega = \omega_3 - \omega_1$, $\Delta z = z_3 - z_1$ is $\Delta m \Delta\omega \Delta z\, E^{\pm}(m_2, \omega_2, z_2, t)$, where $E^{\pm}(m, \omega, z, t)$ is the vertical wavenumber–frequency energy density of either the upward (+) or downward (−) propagating wave field, and Δm, $\Delta\omega$, and Δz are assumed to be small. The time rate of change of energy density in the volume,

$$\Delta m \Delta\omega \Delta z \partial[E^{\pm}(m_2, \omega_2, z_2, t)]/\partial t,$$

is balanced by the difference of energy fluxes through the surfaces defined by $z = z_1$ and $z = z_3$,

$$[C_{gz}(m, \omega)E^{\pm}(m, \omega, z, t)]\Delta m \Delta\omega,$$

where $|C_{gz}| = (\omega^2 - f^2)(N^2 - \omega^2)/\omega m(N^2 - f^2)$ is the vertical group velocity; the difference of downscale spectral transports of energy $F^{\pm}(m, \omega, z, t)\Delta z \Delta\omega$ through the surfaces at $m = m_1$ and $m = m_3$; the dif-

ference of spectral transports in the frequency domain across $\omega = \omega_1$ and $\omega = \omega_3$, $G^{\pm}(m, \omega, z, t)\Delta m\Delta z$; and local energy sources (S_o) or sinks (S_i) within the volume, $\Delta m\Delta z\Delta\omega(S_o^{\pm} - S_i^{\pm})$:

$$\Delta m\Delta\omega\Delta z\frac{\partial E^{\pm}(m_2, \omega_2, z_2, t)}{\partial t} \pm \Delta m\Delta\omega C_{gz}(m_2, \omega_2, z_1)E^{\pm}(m_2, \omega_2, z_1, t) \mp \Delta m\Delta\omega C_{gz}(m_2, \omega_2, z_3)E^{\pm}(m_2, \omega_2, z_3, t)$$
$$+ \Delta\omega\Delta zF^{\pm}(m_1, \omega_2, z_2, t) - \Delta\omega\Delta zF^{\pm}(m_3, \omega_2, z_2, t) + \Delta m\Delta zG^{\pm}(m_2, \omega_1, z_2, t) - \Delta m\Delta zG^{\pm}(m_2, \omega_3, z_2, t)$$
$$= \Delta m\Delta z\Delta\omega(S_o^{\pm} - S_i^{\pm}). \tag{9}$$

Dividing by $\Delta m\Delta\omega\Delta z$ and taking the limit as Δm, $\Delta\omega$, and Δz approach zero results in:

$$\frac{\partial E^{\pm}(m, \omega)}{\partial t} \pm \frac{\partial[C_{gz}(m, \omega)E^{\pm}(m, \omega)]}{\partial z} + \frac{\partial F^{\pm}(m, \omega)}{\partial m} + \frac{\partial G^{\pm}(m, \omega)}{\partial \omega} = [S_o^{\pm}(m, \omega) - S_i^{\pm}(m, \omega)], \tag{10}$$

where C_{gz} has been assumed to be positive definite. The convention here is that both wavenumber and frequency are positive. The direction of propagation or sign of a spatial flux is given explicitly. The group velocity belongs inside the spatial divergence operator in this representation. There is no intrinsic limitation to the number of spatial dimensions referenced by the kinematic argument resulting in (10). In general, one can infer conservation statements of the form

$$\partial_t E(\mathbf{k}) + \nabla \cdot [\mathbf{C_g}E(\mathbf{k})] + \nabla_{\mathbf{k}} \cdot \mathbf{F}(\mathbf{k})$$
$$= S_o(\mathbf{k}) - S_i(\mathbf{k}). \tag{11}$$

Equation (10) describes the evolution of the vertical wavenumber–frequency energy density as a function of depth and time. The fluxes $F^{\pm}(m, \omega)$ and $G^{\pm}(m, \omega)$ represent transfers of wave energy in vertical wavenumber–frequency space resulting from a variety of physical mechanisms, including wave–wave interactions, buoyancy scaling, and wave–mean flow interactions. Of exclusive interest here are wave–wave interactions. The source–sink terms on the right-hand side of (10) can represent either the production and dissipation of energy or the transfer of energy between waves having different wavenumber and frequency. In the oceanic context, wave generation typically occurs at the boundaries. In such cases the energy sources enter through boundary conditions rather than having an $S_o^{\pm}(m, \omega)$ representation.

Dissipation is viewed here as being implicitly represented in (10) through high-wavenumber transports $F^{\pm}(m, \omega)$ rather than having an explicit $S_i^{\pm}(m, \omega)$ representation. Integrating over the vertical wavenumber and frequency domains ($\int_0^{\infty}\int_f^N d\omega\, dm$) and then summing the up–down spectra ($E \equiv E^+ + E^-$) returns

$$\frac{\partial E_{\text{total}}}{\partial t} + \frac{\partial E_{\text{flux}}}{\partial z} = \int_0^{\infty}\int_f^N S_o(m, \omega)\, d\omega\, dm$$
$$- \int_f^N F(m = \infty, \omega)\, d\omega, \tag{12}$$

in which no-flux boundary conditions [$F(m = 0, \omega) = 0$, $G(m, \omega = f) = 0$ and $G(m, \omega = N) = 0$] have been invoked. Here E_{total} represents the total energy and E_{flux} the total vertical energy flux. It has been assumed that nonlinear interactions can be written as transports $F(m, \omega)$ and $G(m, \omega)$. The energy transport at high wavenumber is interpreted as representing the rate of dissipation of internal wave energy:

$$(1 - R_f)\int_f^N F(m = \infty, \omega)\, d\omega = \epsilon, \tag{13}$$

in which the flux Richardson number (R_f, $R_f \cong 0.2$) expresses the partitioning of turbulent production into potential energy fluxes and dissipation; see, for example, Gregg (1987).

Transfers associated with resonant interactions have an explicit ($S_o^{\pm} - S_i^{\pm}$) representation. Closures can be developed that lead to expressions for the energy exchange among three waves of the form

$$\frac{\partial}{\partial t}A(\mathbf{k_3}) = \iint d\mathbf{k_1}\, d\mathbf{k_2}\mathbf{T}^{\Sigma}\delta(\mathbf{k_3} - \mathbf{k_1} - \mathbf{k_2})$$
$$\times\ \delta(\omega_3 - \omega_1 - \omega_2)$$
$$\times\ [A(\mathbf{k_1})A(\mathbf{k_2}) - A(\mathbf{k_3})A(\mathbf{k_1}) - A(\mathbf{k_3})A(\mathbf{k_2})]$$
$$+\ 2\mathbf{T}^{\Delta}\delta(\mathbf{k_3} - \mathbf{k_1} + \mathbf{k_2})\delta(\omega_3 - \omega_1 + \omega_2)$$
$$\times\ [A(\mathbf{k_1})A(\mathbf{k_2}) + A(\mathbf{k_3})A(\mathbf{k_1})$$
$$- A(\mathbf{k_3})A(\mathbf{k_2})], \tag{14}$$

in which $\mathbf{T}^{\Sigma}$ and $\mathbf{T}^{\Delta}$ are interaction matrices, $\mathbf{k_i}$ is a 3D wave vector, subscripts are used to distinguish the three waves, and the δ functions represent the resonance conditions (Müller et al. 1986). Aside from concerns about the formal validity of the assumptions required to produce (14), one can build little intuition from numerical evaluation of (14). Any synthetic treatment that seeks to understand how generation, propagation, nonlinearity, wave breaking, and boundary conditions conspire to shape the observed wave field pragmatically requires

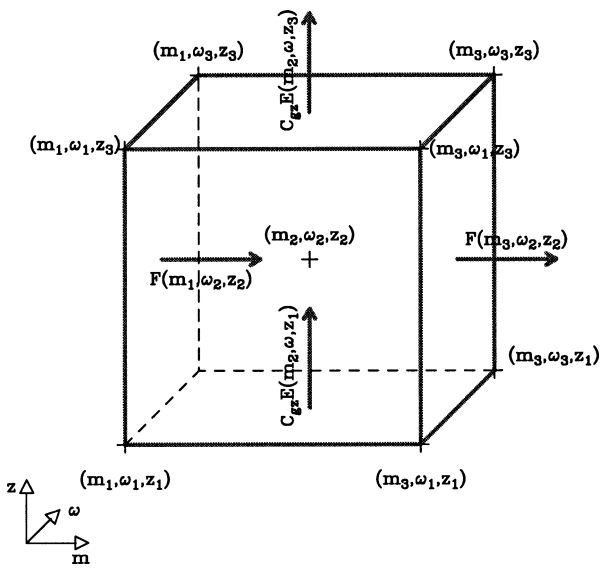

FIG. 2. A schematic of the energy balance for the vertical wavenumber energy spectrum, E, at vertical wavenumber m_2 and vertical coordinate z_2. The vertical flux of energy density is $C_{gz}E$, and transfers of energy to smaller scales are represented by F. Transports of energy in the frequency domain, G, are normal to the forward face but are not depicted.

an approximate treatment of (14). An obvious course of action is to represent (14) in terms of fluxes F and G (10).

In the next section, flux representations for wave–wave interaction transports are developed in the context of a spatially homogeneous wave field:

$$\frac{\partial E(m,\ \omega)}{\partial t} + \frac{\partial F(m,\ \omega)}{\partial m} + \frac{\partial G(m,\ \omega)}{\partial \omega} = S_o(m,\ \omega), \quad (15)$$

in which transfers of energy between waves are assumed to be represented in terms of $F(m,\ \omega)$ and $G(m,\ \omega)$. Thus, the right-hand side of (15) represents only wave generation processes.

c. *A heuristic assessment*

In what follows, input of energy into the internal wave field is assumed to occur at vertical scales of 100s to 1000s of meters by unspecified processes (e.g., by the wind or tides). The removal of energy by wave breaking is assumed to occur at small scales (smaller than 1 m). Thus, there is an intermediate range of scales well removed from dissipation and forcing where energy is assumed to be transferred between scales via the agency of nonlinear interactions between internal waves.

The perspective here is that the oceanic internal wave field in this intermediate range reflects the character of the nonlinear interactions. In the context of (15), this implies

$$O[\partial_t E(m,\ \omega),\ S_o(m,\ \omega)] \leq O[\partial_m F(m,\ \omega),\ \partial_\omega G(m,\ \omega)] \ll O[F(m,\ \omega)/m,\ G(m,\ \omega)/\omega],$$

in which O denotes the order of magnitude. In the following, a stationary spectrum is sought for which $\partial_m F(m,\ \omega) = \partial_\omega G(m,\ \omega) = 0$ (energy density executes a nondivergent cascade). Dimensional analysis and the identification of $\int_f^N F(m,\ \omega)\, d\omega$ with ϵ within the cascade regime will be used.

1) THE STATIONARY SPECTRUM

The process of identifying the stationary spectrum using dimensional analysis is straightforward if there are single time and length scales. For instance, in the inertial subrange of 3D turbulence, the one-dimensional energy spectrum $E(\kappa)$ depends only on the total wavenumber $\kappa = |\mathbf{k}|$ [the wave vector is $\mathbf{k} = (k,\ l,\ m)$, with m being vertical wavenumber] and the transport of energy to smaller scales (assumed to be nondivergent and hence given by the rate of dissipation of turbulent kinetic energy ϵ) so that

$$E(\kappa) \propto a\epsilon^{1/q}\kappa^{-p}, \quad (16)$$

where the exponent p is the stationary power law, q is an exponent relating the spectral density to the transport, and a is an $O(1)$ constant. Since $E(\kappa)$ has the dimensions of length^3/time^2 and ϵ has dimensions of length^2/time^3, $p = 5/3$ and $1/q = 2/3$ out of dimensional necessity.

Unlike the Kolmogorov cascade in which the time scale is given by the transport ϵ and the length scale κ^{-1}, there are several time scales to consider in the internal wave problem. Wave frequency is likely to be most important, but other parameters (such as f and N) and nondimensional combinations could enter. Because of this multiplicity, there are a number of points of ambiguity.

These ambiguities are resolved through a heuristic approach. In a heuristic study, one proceeds along empirical lines using rules of thumb. The rules of thumb followed here are (i) consistency with extant observations and (ii) an assumption that the character of the nonlinearity is not intrinsically related to boundaries in the spectral domain ($\omega = f$, $\omega = N$ and $m = 0$). This assumption is similar to a scale-invariant analysis of (14) in Lvov and Tabak (2001). Here, the assumption that spectral boundaries are not intrinsically related to the cascade dictates that nondimensional ratios of ω/N be interpreted as an aspect ratio,

$$\omega/N \cong (\omega^2 - f^2)^{1/2}/N = k_h/m.$$

The buoyancy frequency enters through the basic kinematic scaling for internal waves in variable stratification; $E(m,\ \omega) \propto N$ under the WKB approximation. With this requirement, an assumption that the stationary spectrum depends upon the (nondivergent) transport $\int_f^N F(m,\ \omega)\, d\omega$ and the postulate that the only important length and time scales determining the energy density at a vertical wavenumber m and frequency ω are $1/m$ and $1/\omega$, dimensional arguments are used to evaluate the grouping:

$$E(m, \omega) \propto N\epsilon^{1/q}m^{-p}\omega^{-r}. \tag{17}$$

Here $E(m, \omega)$ has the dimensions of length^3/time, ϵ has dimensions of length^2/time^3, m^{-1} has the dimension of length, and N^{-1} and ω^{-1} have the dimension of time. The exponents p and r are the stationary power laws and q is an exponent relating the spectral density to the transport. Solving (17) for the spatial and temporal dimensions returns two relations between three parameters, $3 = 2/q + p$ and $-1 = -1 - 3/q + r$.

Nondimensional groupings involving ϵ, m^2, and time^{-3} in which N, ω, and/or f could represent time^{-1} have also been neglected. By construction, such nondimensional groups would have to occur as the argument of a function, such as $\log(N^3/\epsilon m^2)$, rather than as a power law. The observational database (e.g., Fig. 1) suggests that this nondimensional grouping is of little consequence. But this prejudice may simply be arrived at through ignorance.

Section 2a summarized observational constraints for the relation between ϵ and finestructure parameters. The observations provide solid evidence for a quadratic relationship among ϵ, $m^2E(m)$, and N. The observations are consistent with $q = 2$ and $p = 2$. As $3 = 2/q + p$, the observations are dimensionally consistent with (17). Finally, solving $-1 = -1 - 3/q + r$ for r with $q = 2$ returns $r = 3/2$: $E(m, \omega) \propto N\omega^{-3/2}$. Since I assume the character of the nonlinearity is not related to boundaries in the spectral domain, the factor N/ω is interpreted as $N/(\omega^2 - f^2)^{1/2}$ and the stationary spectrum is given by

$$E(m, \omega) \propto N\epsilon^{1/2}m^{-2}\omega^{-1/2}(\omega^2 - f^2)^{-1/2}. \tag{18}$$

This differs from the empirical GM spectrum: $E_{\mathrm{GM}}(m, \omega) \propto Nm^{-2}\omega^{-1}(\omega^2 - f^2)^{-1/2}$.

2) Vertical wavenumber transport $F(m, \omega)$

In this effort to define the energy transport through the vertical wavenumber domain, $F(m, \omega)$, dimensional analysis and the observed relation between ϵ and $E(m)$ provide the guidance that

$$\int_f^N F(m, \omega)\, d\omega \propto \tau(f, N)m^4E(m)^2, \tag{19}$$

where τ is an undefined function of f and N having dimensions of time. A point of ambiguity is how to represent $F(m, \omega)$ in terms of $E(m)$ and/or $E(m, \omega)$ given the integral relation in (19). Since (6) demonstrates a remarkable ability to summarize the observations, the heuristic approach undertaken here suggests

$$F(m, \omega) = AH(f, \omega, N)m^4E(m, \omega)E(m), \tag{20}$$

in which A is a nondimensional constant and $H(f, \omega, N)$ is a factorization of the scaling associated with the temporal dimension. The specific representation of $F(m, \omega)$ in terms of the energy spectrum is local in the vertical wavenumber domain and nonlocal in the frequency domain. It states that the transport at (m, ω) is proportional to the product of the energy density $E(m, \omega)$ and the energy at m integrated over all frequencies. The semi-empirical transport (20) differs from (6) in the vertical wavenumber domain through the approximation $\int_0^m m'^2E_k(m')\, dm' \cong m^3E_k(m)$. This expression is exact for a white shear spectrum. Based upon results for nonwhite shear spectra presented in Polzin et al. (1995), one can infer little difference in the predictive capability of (20) and (6).

In order to specify $H(f, \omega, N)$, the heuristic approach again motivates an appeal to the observations, which dictate a quadratic dependence of $F(m)$ upon buoyancy frequency and linear dependence upon Coriolis frequency for the GM wave field. That is,

$$Am^4E_{\mathrm{GM}}^2(m)\int_f^N H(f, \omega, N)\Omega_{\mathrm{GM}}(\omega)\, d\omega \equiv \epsilon_{\mathrm{GM}} \propto fN^2, \tag{21}$$

with $E_{\mathrm{GM}}(m, \omega) = E_{\mathrm{GM}}(m)\Omega_{\mathrm{GM}}(\omega)$. Given $m^2E_{\mathrm{GM}}(m) = 0.075N^2$ (m s^{-2}) at high m and

$$\Omega_{\mathrm{GM}}(\omega) = \frac{2f}{\pi}\frac{1}{\omega(\omega^2 - f^2)^{1/2}},$$

it is straightforward to infer that the observed f dependence requires eliminating the inertial cusp in the integrand of (21):

$$H(f, \omega, N) = (\omega^2 - f^2)^{1/2}/N^2 \tag{22}$$

is consistent with $\epsilon \propto fN^2$ to within a logarithmic correction. The factor $(\omega^2 - f^2)^{1/2}/N$ represents an aspect ratio $[(\omega^2 - f^2)^{1/2}/(N^2 - \omega^2)^{1/2}$ including nonhydrostatic effects], which cannot be inferred from dimensional arguments alone. The transport is therefore prescribed as

$$F(m, \omega) = Am^4N^{-1}\phi(\omega)E(m, \omega)E(m), \tag{23}$$

with $A = 0.10$ and

$$\phi(\omega) = [(\omega^2 - f^2)/(N^2 - \omega^2)]^{1/2}.$$

The functional representation denoted by ϕ implies increasing transport with increasing wave frequency, as suggested by the observations. The transport magnitude set by the nondimensional constant A is taken from the validation studies of Polzin et al. (1995) and Gregg (1989), who tested similar expressions [section 2a and, in particular, (6)]. Equation (6) is equivalent to the parameterization published in Henyey et al. (1986), and (6) can be obtained from that work by simply assuming energy transports $F(m)$ are nondivergent for the GM vertical wavenumber spectrum. This formulation of Henyey et al. (1986) is written here in such a manner as to facilitate interpretation of past observational studies relative to (19).

3) Frequency domain transport $G(m, \omega)$

Unlike the transport in the vertical wavenumber domain, $F(m)$, there are no direct observations to quan-

titatively constrain the transport in the frequency domain, $G(m, \omega)$. One can, however, infer that, to the degree variations in oceanic spectra can be explained by a simple buoyancy scaling and can reasonably be described as separable, there is likely a basic similarity in the following:

- the functional representation of the quadratic nonlinearity,
- a relaxation to the stationary power law for $\omega \gg f$, $E(m, \omega) \propto \omega^{-3/2}$.

Thus I assume the representation

$$G(m, \omega) = Bm^3\vartheta(\omega)E(m, \omega)E(m). \tag{24}$$

The factor ϑ is nondimensional and requires an $\omega^{3/2}$ dependence at high wavenumber. Consistent with the principle that the cascade not be intrinsically linked to boundaries in the spectral domain, a nondimensional expression is accomplished through the argument ω/N and this argument is interpreted as an aspect ratio:

$$\vartheta(\omega) = \left(\frac{\omega^2 - f^2}{N^2}\right)^{3/4}. \tag{25}$$

As written, $G(m, \omega)$ represents a relaxation to a spectrum with slightly increased inertial peak relative to (18). Ratios of kinetic to potential energy are about 2 for the stationary spectrum, 3 for the GM spectrum, and 4 for a frequency spectrum having the inverse functional dependence as $G(m, \omega)$, $(\omega^2 - f^2)^{-3/4}$. Away from topography, observed ratios are typically 5–10 at $m =$ 0.01 cpm and 3 at 0.1 cpm, and tend to values of 1–2 at smaller vertical wavelengths (Polzin et al. 2003). Polzin et al. (2003) interpret this decrease as being associated with increasing levels of quasi-permanent density finestructure rather than a relative increase of high-frequency waves. While the difference between the frequency dependence of the stationary spectrum (18) and the flux law $G(m, \omega)$ is unsettling, $G(m, \omega)$ is not obviously inconsistent with finescale observations. Regardless, the transport $G(m, \omega)$ is nonzero for $f < \omega < N$. Preliminary analysis of extant data suggests the nondimensional constant B is positive and smaller than A. Energy transport is to higher frequency, which is consistent with low-frequency sources. In contrast, energy transports are to lower frequency in the dynamical balance of McComas and Müller (1981b). I anticipate future studies will suggest improvements for $G(m, \omega)$.

4) BOUNDARY CONDITIONS ON THE TRANSPORT SCHEME

Unlike the cascade in the vertical wavenumber domain, in which the transport $F(m = 0, \omega) = 0$ simply because there is no internal wave energy at $m = 0$ and the transport $F(m = \infty, \omega)$ is accommodated by a nonspecified energy sink, freely propagating waves are not allowed outside of the frequencies of f and N: the cascade in the frequency domain is thus inhibited by the boundaries at $\omega = f$ and $\omega = N$. With the stipulated $\vartheta(\omega)$ (25), $G(m, f) = 0$. The remaining issue is how to prescribe the transports such that $G(m, N) = 0$. This is accomplished here by invoking the hydrostatic approximation in (24) but not in (23). Thus vertical wavenumber domain transports become much more efficient than frequency domain transports as ω approaches N and the combination of (23) with (24) assures that $E(m, N) = 0$. While producing a physically reasonable result at $\omega = N$, the dispersion relation used here assumes a constant N profile. Turning point dynamics might obviate such arguments. Again, future studies will suggest improvements.

5) SUMMARY

Dimensional analysis was used to specify functional forms for the spectral transports through the vertical wavenumber and frequency domains. The transports were written such that they yield nondivergent fluxes for power laws of m^{-2} and $\omega^{-3/2}$. As written, the flux laws produce energy transports to higher wavenumber and frequency. The transports are quadratically dependent upon spectral level and buoyancy frequency for the background (GM) internal wave field. Transports in both vertical wavenumber and frequency domains increase with increasing frequency.

3. Momentum conservation

a. Vertical symmetry of finescale spectra

The shear (likewise velocity) spectrum can be decomposed into components that quantify the clockwise (cw) and counterclockwise (ccw) phase rotation of the shear vector with depth (Leaman and Sanford 1975). For a single wave, this rotary decomposition depends upon the wave and Coriolis frequency as

$$\frac{\text{cw}}{\text{ccw}} = \frac{(\omega + f)^2}{(\omega - f)^2}, \tag{26}$$

with an excess (deficit) of ccw phase rotation denoting an excess (deficit) of upward-propagating energy in the Northern Hemisphere. The opposite applies to the Southern Hemisphere. Interestingly, most, if not all, spectra that exhibit a difference between rotary components at large wavelengths are symmetric at smaller scales (Fig. 3). Here the transition between large and small appears to coincide with the vertical wavenumber cutoff m_c (7). At scales smaller than $1/m_c$ the shear spectra roll off, tending toward an m^{-1} dependence (Gargett et al. 1981). This roll off is interpreted as being in response to strong nonlinearity not captured by the closure scheme under consideration.

The data in Fig. 3 are taken from midlatitude regions in the western North Atlantic: one from Mid-Ocean Dynamics Experiment (MODE; Leaman and Sanford

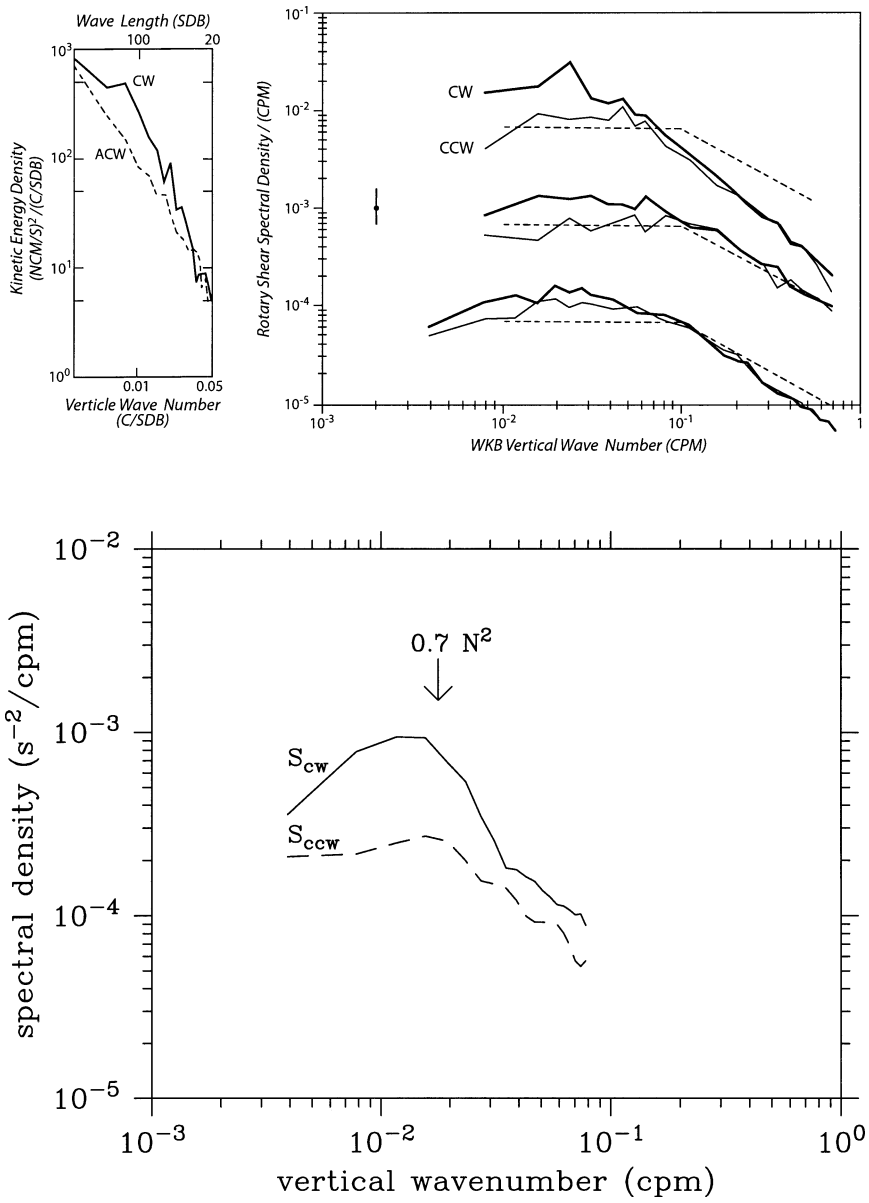

FIG. 3. Rotary spectra from the western North Atlantic. (top left) Kinetic energy spectra from MODE [redrawn from Leaman and Sanford (1975)]; (top right) shear spectra from FASINEX (redrawn from Weller et al. 1991) corresponding to seasonal thermocline, 18° water, and the main thermocline (from top to bottom) are offset by one decade. The dashed lines represent the GM76 spectrum. Data from the upper panels have been buoyancy scaled via WKB stretching to a reference of $N_o = 3$ cph. (bottom) Shear spectra from a Gulf Stream warm core ring (Kunze et al. 1995); the clockwise (cw) spectra tend to lie above the counterclockwise (ccw) in all cases. While difference between the two is apparent at large scales, that difference diminishes with increasing vertical wavenumber.

1975), a second from the Frontal Air–Sea Interaction Experiment (FASINEX; Weller et al. 1991), and a third from a warm core ring of the Gulf Stream (Kunze et al. 1995). Wave–wave interactions may not be the sole agent that can produce a symmetric spectrum. Wave–mean flow interactions are obviously significant for the warm ring data, but the possible role of wave–mean flow interactions in producing a symmetric pattern is not obvious. The MODE data could possibly be explained as the sum of a symmetric background and downward-propagating, near-inertial, internal waves being transported to larger vertical scales by buoyancy scaling with an $N(z)$ profile that decreases with depth. Such an explanation does not suffice for the FASINEX results as those data are averaged in depth bins coinciding with structure in the $N(z)$ profile. Data from the

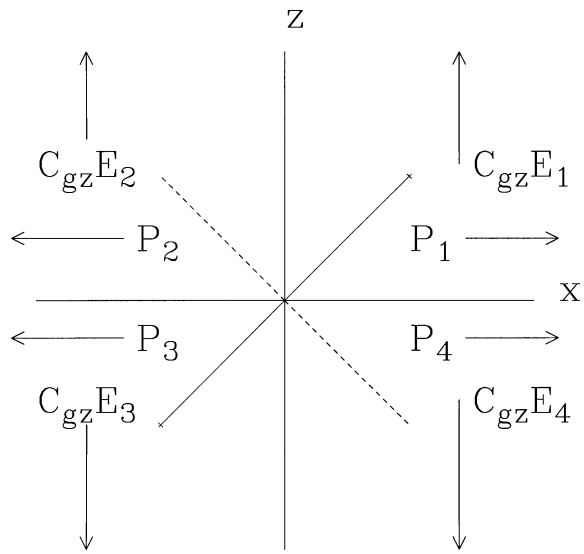

FIG. 4. A schematic depicting the direction of the vertical energy flux ($C_{gz}E$) and horizontal momentum (P) in the (x, z) plane. The (1, 3) and (2, 4) quadrants are coupled through the flux representation of nonlinear transports (33)–(34). The (1, 3) [and (2, 4)] quadrants have oppositely signed wave vectors.

relative N^2 minimum associated with 18° water exhibit a symmetric spectrum at high wavenumber. The symmetric pattern could represent a transition to higher internal wave frequency with higher vertical wavenumber. However, (26) is not a particularly sensitive function of frequency. Analysis of similar vertical profile data from the eastern North Atlantic thermocline (Polzin et al. 2003) suggests that the internal wave field retains its near-inertial character for $m > m_c$, consistent with other finescale observations (Kunze et al. 1990; Anderson 1992). The hypothesis is forwarded that vertical symmetry is linked to momentum conservation issues.

b. Integral constraints

Implicit in this work is the assumption that energy transports are local in the vertical wavenumber domain. Any internally consistent approach requires energy and momentum conservation to be conserved locally. Nonlocal closures in the resonant interaction approximation are, however, certainly possible. See, for example, the induced diffusion approximation described in McComas and Bretherton (1977).

The issue of momentum conservation arises for spatially inhomogeneous wave fields. One could, in general, consider the evolution of a three-dimensional energy spectrum $E(m, \omega, \theta)$ in vertical wavenumber (m), frequency (ω), and horizontal azimuth (θ) in 3D space and time. A simple result can be obtained by considering the vertically asymmetric case for a single horizontal azimuth. To be definite, the azimuth coincides with the eastward coordinate. The evolution of the energy spectrum $E(m, \omega)$ is defined by

$$\frac{\partial E^{\pm}(m,\omega)}{\partial t} \pm \frac{\partial[C_{gz}E^{\pm}(m,\omega)]}{\partial z} + \frac{\partial F_e^{\pm}(m,\omega)}{\partial m} + \frac{\partial G_e^{\pm}(m,\omega)}{\partial \omega} = [S_o^{\pm}(m,\omega) - S_i^{\pm}(m,\omega)]_e, \tag{27}$$

where C_{gz} has been assumed to be positive definite. The convention has been taken that both wavenumber and frequency are positive. The direction of vertical propagation is indicated with the superscript notation, and the sign of a spatial flux is given explicitly. Subscripts of e are used to distinguish energy fluxes from momentum fluxes below. A similar conservation statement can be had for wave momentum $\mathbf{P} = \mathbf{k}E/\omega$; that is,

$$\pm\frac{\partial \mathbf{P}^{\pm\pm}(m,\omega)}{\partial t} \pm \pm \frac{\partial[C_{gz}\mathbf{P}^{\pm\pm}(m,\omega)]}{\partial z} \pm \frac{\partial \mathbf{F}_p^{\pm\pm}(m,\omega)}{\partial m} \pm \frac{\partial \mathbf{G}_p^{\pm\pm}(m,\omega)}{\partial \omega} = [\mathbf{S}_o^{\pm\pm}(m,\omega) - \mathbf{S}_i^{\pm\pm}(m,\omega)]_p, \tag{28}$$

in which $\mathbf{F}_p^{\pm\pm}(m, \omega)$ and $\mathbf{G}_p^{\pm\pm}(m, \omega)$ are flux representations for the spectral transport of momentum and $\mathbf{k} = (k, l, m)$ is the wave vector. Note the introduction of an additional $\pm$ denoting the sign of the horizontal wavenumber and, hence, sign of the horizontal momentum. The internal wave frequency determines the angle of propagation with respect to the vertical. In any vertical plane there are four physically distinct waves for each vertical wavenumber and frequency.

Rather general integral constraints can be derived from (27) and (28). In the manipulations below, note that (27) and (28) represent spectral balances, not wavepacket balances. Thus m and ω are independent of z, permitting the interchange of orders of integration and application of simple rules for the inclusion of independent variables within partial differentiation operations.

Consider trying to obtain the momentum balance (28) from the energy equation (27) for an upward- and eastward-propagating (++) spectrum. Multiplication of (27) by $k/\omega = \beta(\omega)m$ with $\beta = [(\omega^2 - f^2)/\omega^2(N^2 - \omega^2)]^{1/2}$ returns

$$\frac{\partial P^{++}(m,\omega)}{\partial t} + \frac{\partial[C_{gz}P^{++}(m,\omega)]}{\partial z} + m\frac{\partial[\beta F_e^{++}(m,\omega)]}{\partial m} + \beta\frac{\partial[mG_e^{++}(m,\omega)]}{\partial \omega} = 0. \tag{29}$$

Integration of (29) returns

$$\frac{\partial P_{\text{total}}^{++}}{\partial t} + \frac{\partial P_{\text{flux}}^{++}}{\partial z} = -\int_f^N F_p^{++}(m = \infty, \omega)\, d\omega + \int_0^\infty \int_f^N \beta(\omega)F_e^{++}(m,\omega)\, dm\, d\omega + \int_0^\infty \int_f^N mG_e^{++}(m,\omega)\frac{\partial\beta(\omega)}{\partial\omega}\, dm\, d\omega, \tag{30}$$

where P_{total}^{++} is the total momentum and P_{flux}^{++} is the total

vertical flux of horizontal momentum of the upward, eastward wave field. In comparison, integration of the momentum equation [(28) with no $S_o^{\pm\pm}(m, \omega) - S_i^{\pm\pm}(m, \omega)$ term] returns

$$\frac{\partial P_{\text{total}}^{++}}{\partial t} + \frac{\partial P_{\text{flux}}^{++}}{\partial z} = -\int_f^N F_p^{++}(m = \infty, \omega)\, d\omega. \quad (31)$$

Clearly, either the identification of $F_p^{++}(m, \omega)$ as $m\beta(\omega)F_e^{++}(m, \omega)$ and $G_p^{++}(m, \omega)$ as $m\beta(\omega)G_e^{++}(m, \omega)$ are wrong, or a flux representation as in (27) does not conserve momentum.

c. A closure scheme

It is possible to construct a $(S_o^{\pm} - S_i^{\pm})_e$ representation that serves to conserve momentum while still conserving energy. The trick is facilitated by realizing that, while energy is positive-definite, momentum is a signed quantity. The conservation of momentum can be guaranteed by backscattering wave energy into an oppositely signed wave vector at a rate in proportion to the spectral transports so that no net energy is generated or dissipated. The best demonstration is by example. Consider the energy and momentum balances for waves in each of four quadrants (Fig. 4):

$$\frac{\partial E^{\pm\pm}(m, \omega)}{\partial t} \pm \frac{\partial [C_{gz}E^{\pm\pm}(m, \omega)]}{\partial z} + \frac{\partial F_e^{\pm\pm}(m, \omega)}{\partial m} + \frac{\partial G_e^{\pm\pm}(m, \omega)}{\partial \omega} = [S_o^{\pm\pm}(m, \omega) - S_i^{\pm\pm}(m, \omega)]_e,$$

$$\pm\frac{\partial P^{\pm\pm}(m, \omega)}{\partial t} \pm \pm \frac{\partial [C_{gz}P^{\pm\pm}(m, \omega)]}{\partial z} \pm \frac{\partial F_p^{\pm\pm}(m, \omega)}{\partial m} \pm \frac{\partial G_p^{\pm\pm}(m, \omega)}{\partial \omega} = 0. \quad (32)$$

The convention that the momenta $P^{\pm\pm}(m, \omega)$ are positive-definite has been adopted, and the sign of the momentum is given explicitly. If the source–sink terms for the energy balances are judiciously chosen, one can conserve both the energy and the momentum of this coupled system. A judicious choice is to add zero. For example, if the first and third quadrants are coupled as

$$[S_o^{++}(m, \omega) - S_i^{++}(m, \omega)]_e = \frac{1}{2m}[F_e^{--}(m, \omega) - F_e^{++}(m, \omega)] + \frac{1}{2}\frac{[G_e^{--}(m, \omega) - G_e^{++}(m, \omega)]}{\beta}\frac{\partial \beta}{\partial \omega} \quad \text{and} \quad (33)$$

$$[S_o^{--}(m, \omega) - S_i^{--}(m, \omega)]_e = \frac{1}{2m}[F_e^{++}(m, \omega) - F_e^{--}(m, \omega)] + \frac{1}{2}\frac{[G_e^{++}(m, \omega) - G_e^{--}(m, \omega)]}{\beta}\frac{\partial \beta}{\partial \omega}, \quad (34)$$

then total energy has been conserved:

$$\frac{\partial [E^{++}(m, \omega) + E^{--}(m, \omega)]}{\partial t} + \frac{\partial \{C_{gz}[E^{++}(m, \omega) - E^{--}(m, \omega)]\}}{\partial z} + \frac{\partial [F_e^{++}(m, \omega) + F_e^{--}(m, \omega)]}{\partial m}$$

$$+ \frac{\partial [G_e^{++}(m, \omega) + G_e^{--}(m, \omega)]}{\partial \omega} = 0. \quad (35)$$

The momentum balance of the coupled system [$m\beta$ times the upward, eastward ($++$) energy balance and $-m\beta$ times the downward, westward ($--$) energy balance] is simply

$$\frac{\partial [P^{++}(m, \omega) - P^{--}(m, \omega)]}{\partial t} + \frac{\partial \{C_{gz}[P^{++}(m, \omega) + P^{--}(m, \omega)]\}}{\partial z} + \frac{\partial \{m\beta(\omega)[F_e^{++}(m, \omega) - F_e^{--}(m, \omega)]\}}{\partial m}$$

$$+ \frac{\partial \{m\beta(\omega)[G_e^{++}(m, \omega) - G_e^{--}(m, \omega)]\}}{\partial \omega} = 0. \quad (36)$$

The second and fourth quadrants can be coupled to produce a similar result.

The coupling proposed here can be interpreted as a backscattering process. Backscattering in the resonant interaction approximation (a.k.a. elastic scattering) is the transfer of energy between upward- and downward-propagating waves having similar horizontal wavenumber and vertical wavenumber of opposite sign but similar magnitude (e.g., quadrants 1 and 4 in Fig. 4). It is a process that tends to equalize the vertical *fluxes* of

energy and horizontal momentum of the two waves. The total horizontal momentum of the two waves is conserved.

Backscattering in this present flux representation is the transfer of energy between two waves of similar but oppositely signed wave vectors. The rate of this transfer is set by the transport of energy to smaller scales, which on its own tends to increase momentum. Backscattering in the flux representation cancels this tendency and acts to equalize the horizontal momentum and vertical *flux* of energy of the two waves.

Backscattering in this flux representation and in the RIA are distinct. In particular, horizontal momentum in the flux representation cannot be conserved by exchanging quadrant 4 for quadrant 3 in Fig. 4. Exchanging quadrant 2 for quadrant 3 can conserve horizontal (but not vertical) momentum. Coupling quadrants 1 and 2 would not result in the transfer of energy between upward- and downward-propagating waves and is inconsistent with the apparent symmetry of the finescale wave field discussed in section 5. The coupling of quadrants 1 and 3 is consistent with the issue of diagonal dominance discussed in Carnevale and Fredricksen (1983), who found that coupling between quadrants 1 and 2 is the mechanism that supports a vertical mass flux, that is, wave breaking. In contrast, the closure scheme presented here is not intended to describe the effects of wave breaking and strong nonlinearity at vertical wavenumbers $m > m_c$.

The central result of this section is that a general flux representation of transfers associated with wave–wave interactions that conserves both momentum and energy can be obtained. The conservation of momentum can be guaranteed by the backscattering of wave energy at a rate in proportion to the spectral transports. In terms of an upward–downward decomposition, a general expression is

$$\frac{\partial E^{\pm}(m,\omega)}{\partial t} \pm \frac{\partial[C_{gz}E^{\pm}(m,\omega)]}{\partial z} + \frac{\partial F_e^{\pm}(m,\omega)}{\partial m} + \frac{\partial G_e^{\pm}(m,\omega)}{\partial \omega} = \frac{1}{2m}[F_e^{\mp}(m,\omega) - F_e^{\pm}(m,\omega)] + \frac{1}{2}\frac{[G_e^{\mp}(m,\omega) - G_e^{\pm}(m,\omega)]}{\beta}\frac{\partial \beta}{\partial \omega}. \quad (37)$$

Only slight modification of (23) and (24) is required in order to account for possible asymmetry: $E(m, \omega)$ is simply replaced with $E^{\pm}(m, \omega)$.

4. A brief demonstration of the transport scheme's utility as a prognostic model

a. Observations

An independent dataset is examined below to demonstrate the transport scheme's utility as a prognostic model.

Observations obtained from the Brazil Basin as part of an anthropogenic tracer release experiment (Polzin et al. 1997; Ledwell et al. 2000) provided the initial motivation for this study. In those data, turbulent dissipation is orders of magnitude larger above rough topography associated with the Mid-Atlantic Ridge than above the smooth abyssal plain. Enhanced velocity finestructure occurs in conjunction with the increased dissipation in stratified water removed from the bottom boundary, implicating internal wave breaking as the source of turbulent energy. Polzin et al. (1997) proposed that the elevated finestructure levels were associated with the local generation of internal waves at tidal frequencies having horizontal scales characteristic of the topographic roughness ($\leq$1000 m). Providing the quantitative link between the fine- and microstructure observations, though, required the development of this heuristic description of internal wave dynamics. A brief application of the model to those data is presented below. A more detailed study is presented in Polzin (2004).

The observed shear spectrum near the bottom boundary is peaked at vertical wavelengths of about 100 m. Away from the bottom boundary, observed shear spectra from the Brazil Basin appear to relax to uniform levels with the substantive change being the decay of the spectral peak (Fig. 5). Lower spectral levels at larger vertical wavelengths are consistent with a spectral model of baroclinic tide generation (Bell 1975) and the topographic roughness (Polzin 2004). Lower spectral levels at smaller wavelengths are likely to be associated with the effects of strong nonlinearity and/or wave breaking.

Near the spectral peak the difference between cw and ccw spectra is largest; the difference is negligible at higher wavenumber. The buoyancy profile in this study area decreases weakly with increasing height above bottom, implying small transports associated with buoyancy scaling. Thus, the observed vertical symmetry is interpreted as representing a balance between upward- and downward-propagating internal waves in response to nonlinearity.

Such features are qualitatively consistent with the proposed flux representation. The transport representation (23) implies that deviations from the stationary spectrum, presumably associated with boundary sources, are relaxed back to the stationary form in the absence of forcing. As part of the relaxation, a decay of the spectral level will occur in response to downscale energy transports associated with nonlinearity. In addition, the scattering of waves back toward the boundary associated with the right-hand side of (37) will tend to create a vertically symmetric wave field at smaller scales.

b. A simplification

Much intuition about the spatial decay problem can be gained by ignoring the frequency domain transfers $G(m, \omega)$. While certainly an idealization, this is far less restrictive than might first appear. With regard to the

directional evolution of the wave field, in the hydrostatic nonrotating approximation,

$$\frac{1}{2}\frac{[G_e^{\mp}(m,\ \omega) - G_e^{\pm}(m,\ \omega)]}{\beta}\frac{\partial\beta}{\partial\omega} = 0. \qquad (38)$$

That is, regardless of the specification for $G_e^{\pm}(m,\ \omega)$, momentum conservation does not result in a backscattering of wave energy for $f^2 \ll \omega^2 \ll N^2$. Moreover, the spatial and temporal evolution of the vertical wavenumber spectrum (other than that associated with the backscattering of waves to conserve momentum) does not explicitly depend upon $G_e^{\pm}(m,\ \omega)$. This result can be obtained by integrating (37) over the frequency domain and applying boundary conditions that $G_e^{\pm}(m,\ \omega = f) = G_e^{\pm}(m,\ \omega = N) = 0$:

$$\frac{\partial E^{\pm}(m)}{\partial t} \pm \frac{\partial\left[\int_f^N C_{gz}(m,\ \omega)E^{\pm}(m,\ \omega)\ d\omega\right]}{\partial z} + \frac{\partial F_e^{\pm}(m)}{\partial m}$$
$$= \frac{1}{2m}[F_e^{\mp}(m) - F_e^{\pm}(m)] + \frac{1}{2}\int_f^N \frac{[G_e^{\mp}(m,\ \omega) - G_e^{\pm}(m,\ \omega)]}{\beta}\frac{\partial\beta}{\partial\omega}\ d\omega. \qquad (39)$$

Note further that the frequency dependence of the group velocity cancels that of $F_e^{\pm}(m,\ \omega)$ for $f^2 \ll \omega^2 \ll N^2$, and so, for steady solutions, $E(m)$ does not depend upon the frequency distribution of the bottom boundary condition.

c. Results

The observed pattern of relaxation and vertical symmetry compares reasonably well with a numerical solution of (37) (Fig. 5). The time-dependent version of (37) with the closure (23) and $G^{\pm}(m,\ \omega) = 0$ was solved using a simple upwind difference scheme. The bottom boundary condition was handled by specifying the difference between $E^{+}(m)$ and $E^{-}(m)$ at $z = 0$. This difference represents a source of wave energy at the bottom boundary that was assumed to have a peaked shear spectrum. The input function was taken as an approximate representation of Bell's (1975) internal tide generation model using a barotropic tidal amplitude of 2 cm s^{-1} and topographic spectral parameters obtained from Goff (1992). See Polzin (2004) for further details. No scattering transform was employed (i.e., downward-propagating waves are considered to reflect as from a flat bottom). A no-flux surface boundary condition was used. The frequency spectrum was represented as a delta function, $E^{\pm} = E^{\pm}(m)\delta(\omega - \omega_o)$, with $\omega_o = 1.4025 \times 10^{-4}$ s^{-1}. Other environmental parameters were $f = -5.3 \times 10^{-5}$ s^{-1} and $N = 1 \times 10^{-3}$ s^{-1}, and a water depth of $H = 4000$ m was assumed. The model was run forward in time from an initial state of rest for 200 days, at which point the energy balance was in approximate statistical equilibrium.

An upward-propagating semidiurnal tide at the latitude of the Brazil Basin mixing study would exhibit a cw/ccw ratio of 5. Ratios of 2–3 are observed at vertical wavelengths of 200–250 m (Fig. 5), 100–2100 m above the bottom. At larger wavelengths a difference of about 50% is noted. At large wavelengths, the wave field is sufficiently linear as to reach the surface and reflect, resulting in a near balance between up- and downgoing energy. At smaller wavelengths, the cw/ccw decomposition suggests a vertically symmetric wave field. At small wavelengths, backscattering associated with momentum conservation will tend to create vertically symmetric spectra in a flux formulation.

The point here is not to claim that the numerical solution accurately depicts the oceanic internal wave energy balance in the Brazil Basin. While the degree of agreement between model and data is impressive, this solution is rather idealized. The following patterns are, however, believed to be significant. First, the model response to a peaked input spectrum is a relaxation to a uniform shear spectrum over a decade of wavenumbers $m < m_c$. The transport specification does not capture the strong nonlinearity at wavenumbers $m > m_c$ and thus the model shear spectrum appears uniform rather than tending to roll off in this regime. Second, the backscattering associated with momentum conservation produces model rotary spectra with greatest difference at a wavenumber $m < m_c$. Without the backscattering, the model rotary spectra remain separated at high wavenumber and are inconsistent with the observations.

5. Discussion

Development of the transport scheme was motivated by perceived limitations of the models grounded in first-principle derivations. Specifically, both the RIA and the eikonal representation violate basic assumptions underpinning the respective models. This places very real limitations on their applicability when interpreting observations. On the other hand, both models result in viable parameterizations of ϵ, and it was apparent that a transport scheme could be constructed from those parameterizations. Like Garrett and Munk (1972), much of the effort here is a tool-building exercise. Having concocted such a scheme, the intent is to use the tool to quantify patterns within the oceanic internal wave field and iterativly refine our knowledge about the oceanic internal wave field and internal wave dynamics.

One of the first incongruities brought up by this heuristic approach is contained within the basic construction of the transport scheme. The transport scheme proposed here is local in the vertical wavenumber domain. In contrast, discussion of nonlinearity in the resonant interaction approximation has revolved around three triad classes that are characterized in the limit of extreme

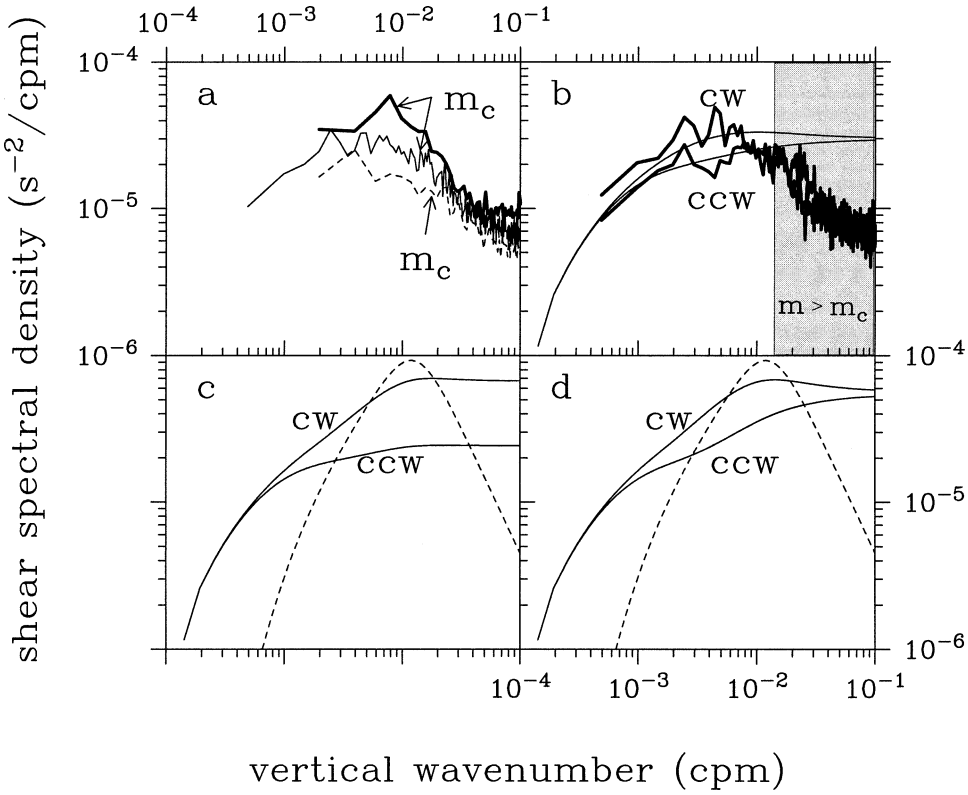

FIG. 5. Observed shear spectra from the Brazil Basin and model estimates. The observations represent an average over the 30 stations that appear in Fig. 3 and east of 18°W in Fig. 2 of Polzin et al. (1997). (a) Shear spectra $m^2E_k(m)$ from a height above bottom (hab) of 100–612 (thick), 100–2148 (thin), and 1636–2148 (dashed) m. The spectrum is peaked near the bottom and relaxes back to a shape that is approximately uniform with wavenumber as the wave field propagates away from the bottom boundary. Cutoff wavenumbers (m_c) for the three spectra are depicted as well. (b) Rotary spectra (100–2148-m hab) for both observations (thick) and model (thin). The clockwise (cw) spectra lie above the counterclockwise (ccw) at the midrange of wavenumbers. The domain is shaded for wavenumbers $m > m_c$. (c), (d) Model output at the bottom boundary. The clockwise spectra are enhanced relative to ccw. The dashed line represents energy input at the bottom-boundary cast in terms of the shear spectrum. Model output in (c) utilizes a closure that does not conserve momentum in which the right-hand side of the energy equation (37) is set equal to zero. Model output (d) correctly incorporates the flux representations (23) and (24) into the right-hand side of (37).

scale separation, and the eikonal representation makes an explicit assumption of scale separation.

If one looks closely and thinks critically, justification both for this tool-building exercise and for a local characterization can be found within the extant theories.

a. The eikonal representation

The eikonal models are based upon infinitesimal-amplitude wave propagation in a background of other internal waves. The infinitesimal-amplitude assumption is made in order to discard quadratic terms of the test waves in the derivation of the test wave Hamiltonian. The eikonal model also invokes a scale separation in order to neglect advection of the background by the test wave. In so doing, one can obtain a linear representation governing test wave propagation for which the intrinsic frequency $\omega = \sigma - \mathbf{k}\cdot\mathbf{U}$ is given by the usual dispersion relation,

$$\omega = \left(\frac{N^2k_h^2 + f^2m^2}{k_h^2 + m^2}\right)^{1/2}.$$

The position and wavenumber of the test wave evolve according to

$$\dot{\mathbf{x}} = \frac{\partial\omega}{\partial\mathbf{k}} + \mathbf{U} \quad \text{and} \quad \dot{\mathbf{k}} = -\frac{\partial\omega}{\partial\mathbf{x}} - \frac{\partial}{\partial\mathbf{x}}\mathbf{U}\cdot\mathbf{k},$$

in which $\mathbf{U}$ is the velocity of the background field. Wave action $A = E/\omega$ is conserved following a ray path and changes in momentum $\mathbf{k}A$ are given by $\dot{\mathbf{k}}A$. Momentum conservation has not been addressed in the context of eikonal wave–wave interaction theories as the wave fields are assumed to be vertically symmetric. Momentum is *not*, in general, conserved, as $\dot{\mathbf{k}}A \neq 0$.

Within this theoretical framework, transport estimates in the eikonal representation are constructed using Monte Carlo methods and tracing test waves through an

ensemble of flows. The energy transport is given as the product of the energy density of the background and an average transport rate $F(m) = \overline{E(m)dm/dt}$. Henyey et al. (1986) considered only Doppler shifting by the horizontal background currents. Sun and Kunze (1999a,b) incorporate Doppler shifting associated with *vertical* currents into the eikonal representation.

Henyey (1984) and Sun and Kunze (1999b) both deduce that the interactions are relatively local in the vertical wavenumber domain. Filtering local vertical wavenumbers from the background results in substantially reduced transports; increasing the background scale by a factor of 2 reduces the transport rates by about a factor of 2. Neither Henyey et al. (1986) nor Sun and Kunze strictly enforce a scale separation in the horizontal domain. This issue is most problematic for Sun and Kunze as the vertical currents included in their simulations have substantially smaller horizontal scales than the horizontal currents and inclusion of the small-horizontal-scale vertical currents is responsible for their large transport estimates. Sun and Kunze (1999a) report that filtering in both vertical and horizontal wavenumber to ensure that the background wave field has similar or larger scales than the test wave eliminates the transports entirely. These model results are quite persuasive evidence for locality. However, they just as persuasively demonstrate that the eikonal representation is far from being a robust summary of the interaction process.

The eikonal representation is limited by the fact that the predicted transports are dominated by interactions of test waves with background waves of similar scale after making an explicit assumption of a scale separation. The scale-separation issue is a fundamental one that goes beyond the validity of the WKB approximation. To the degree that the oceanic wave field is best described as a superposition of finite-amplitude (but not necessarily nonlinear) wave packets rather than a collection of randomly phased, infinitesimal-amplitude waves, identification of the test wave field with the oceanic wave field requires invoking a scale separation in both vertical and horizontal wavenumbers in order to ensure that advection by the background dominates the nonlinearity ($U \gg u$, where U and u represent the amplitude of the background and test wave, respectively). Without a scale separation in both dimensions, the infinitesimal-amplitude approximation is violated for low-frequency test waves and high-frequency background waves ($u \gg U$) if the relative amplitudes of those waves are assumed consistent with the GM prescription. The eikonal representation lacks even the approximate action conservation statement for such interactions. Equivalently, in order to obtain the desired Hamiltonian, a scale separation in both dimensions is required.

b. Resonant interactions

A single plane internal wave is an exact solution of the equations of motion in Eulerian coordinates. This is not, in general, the case for a combination of waves. However, Phillips (1960) noted that two waves with phases ($\mathbf{k_1} \cdot \mathbf{x} - \omega_1 t$) and ($\mathbf{k_2} \cdot \mathbf{x} - \omega_2 t$) will tend to force a third wave with the sum and difference phase:

$$\mathbf{k_1} \pm \mathbf{k_2} = \mathbf{k_3} \quad \text{and} \quad \omega_1 \pm \omega_2 = \omega_3. \tag{40}$$

If the third component is a free wave, that is, if ($\mathbf{k_3}$, ω_3) is a solution to the dispersion relation, then energy is systematically transferred from the first two into the third. Total energy (E) and linear wave momentum ($\mathbf{P} = \mathbf{k}E/\omega$) are conserved by such transfers between the three waves, but not wave action $A = E/\omega$; see, for example, Müller et al. (1986).

The formidable task of estimating the net energy transport accomplished by these wave–wave interactions for a particular region in the wavenumber/frequency domain is facilitated by appealing to well-developed methods in theoretical physics. The resulting transport (or kinetic) equation (14) has been numerically evaluated for the Garrett and Munk spectrum by several groups: Olbers (1976), McComas and Bretherton (1977), and Pomphrey et al. (1980). McComas and Bretherton (1977) introduce three limiting triad classes in an attempt to provide ''physical insight into an otherwise mystifying computational exercise.'' These triad classes have a large separation in frequency and/or wavenumber magnitude between components. That is, the triad classes are defined in the limit of extreme scale separations.

The most important criticism of this approach here is that all three groups derive their Hamiltonian structure by formulating a Lagrangian in Lagrangian coordinates. This approach necessitates a small-amplitude approximation in addition to the assumption of weak nonlinearity that is required to derive the kinetic equation (Müller et al. 1986). In contrast, Lvov and Tabak (2001) derive a Hamiltonian in quasi-Lagrangian (density) coordinates that requires no small-amplitude approximation to construct a kinetic equation. Assuming simply that the interactions are scale invariant, Lvov and Tabak derive high-frequency and wavenumber power laws for the stationary spectrum (18). Rather than emphasizing scale-separated interactions, the conceptual picture in Lvov and Tabak (2001) is a scale-invariant cascade.

The reason for this change in emphasis may go back to the initial derivation in Lagrangian coordinates. Yuri V. Lvov (2003, personal communication) reports differences between the interaction matrices of Lvov and Tabak (2001) and Olbers (1976) on the resonance surface. It is believed that these differences result from the small-amplitude expansion in the Lagrangian analysis being divergent for extreme scale-separated interactions. Thus, much of conventional wisdom regarding the application of resonant interactions to the oceanic internal wave field needs to be reconsidered.

Previous considerations of interaction time scales at small vertical wavelengths suggested that interaction rates were too large for the RIA to be formally valid

(e.g., Müller et al. 1986). Such considerations are likely still a concern with the Lvov and Tabak (2001) formulation. However, the presence of large interaction rates would seem to reinforce the importance of local interactions as resonance broadening becomes a concern first for scale-separated interactions.

c. Summary

One interpretation of the fast interaction rates at high wavenumber predicted by resonant interaction theory (Müller et al. 1986) is that they represent a broadening of the dispersion curves by a simple kinematic Doppler shifting. That frequency-broadening motivated attempts to describe wave–wave interactions with the eikonal representation, which returns the result that interactions are local in the vertical wavenumber domain (fundamentally contradicting the assumption of a scale separation). Understanding of the kinetic equation in its application to oceanic internal waves derives largely from the seminal work of McComas and Bretherton (1977) and McComas and Müller (1981a,b). That approach emphasized the role of scale-separated interactions. A reevaluation of that work appears to be called for.

The scale-invariant analysis of Lvov and Tabak (2001) and the local nature of interactions inferred from the eikonal models suggest the present route: a flux representation based upon dimensional analysis and reliance upon observations to define the basic parameter dependence. How literally should one take the resulting local parameterizations? The reader is reminded that the prototypical cascade model, that of turbulent transfers in the inertial subrange of 3D turbulence, is a useful construct that is not literally true; see, for example, Tennekes and Lumley (1987), their section 8.2.

Goals for future observational efforts include defining (i) the bandwidth required to set up an inertial subrange and (ii) the relative importance of the various theoretical representations. In particular, there may be some nonlocal transport of energy to lower frequency associated with a psi-like mechanism, especially for low-mode internal tides. Moreover, the present transport scheme is not intended to describe the transition to turbulence for $m > m_c$. The inconsistency between the near-inertial cusp of the stationary spectrum and the transport $G(m, \omega)$ points to an unresolved issue.

6. Summary

The work presented herein describes a method for assessing the spatial and temporal evolution of a vertically anisotropic internal wave spectrum. This method invokes a mixed spatial/spectral representation rather than a wave packet or wave train formulation. Nonlinearity is explicitly treated as a flux in the spectral domain. Momentum conservation is attained by transferring energy into an oppositely signed wave vector at a rate proportional to the nonlinear energy transports. Dissipation is implicitly viewed as the end result of nonlinear transfers to high wavenumber.

Dimensional analysis cobbled together with several basic observational constraints and the assumption that nonlinearity is not intrinsically related to boundaries in the spectral domain implies a stationary spectrum of $E(m, \omega) \propto Nm^{-2}\omega^{-3/2}$ at high vertical wavenumber and frequency. This differs from the GM spectrum, for which $E(m, \omega) \propto Nm^{-2}\omega^{-2}$. Flux representations for the spectral transports were inferred using dimensional analysis with energy transports in the vertical wavenumber domain specified to be consistent with extant empirical studies. Energy transports in the frequency domain are to higher frequency. This is consistent with an oceanic spectrum that results from forcing at low frequency and is in the process of relaxing to an $\omega^{-3/2}$ shape. The major sources of internal wave energy are believed to be at low (near-inertial and tidal) frequencies.

A preliminary comparison with data from the abyssal Brazil Basin is encouraging. The proposed transport representation (23) and (24) dictates a relaxation of the shear spectrum to a uniform spectral level and a vertically symmetric wave field at the smallest scales. The apparent relaxation of the observed spectra with height above boundary and vertical symmetry of the spectrum at small scales is replicated by the proposed transport representation in response to a peaked shear spectrum input as a source function at the bottom boundary. There are quantitative differences between the presented numerical solution and observations that require the incorporation of buoyancy scaling in the radiation balance equation, a scattering transform in the bottom boundary condition, and a realistic generation model to further assess the adequacy of the closure scheme.

The proposed flux representation is not a detailed description of the interaction process. It is intended as a simplistic depiction of a local cascade within the fine-scale internal wave regime for anisotropic, inhomogeneous wave fields that retains energy and momentum conservation principles. Rather than seeking a detailed theoretical understanding of nonlinear internal wave interactions, the attempt here is to develop a *relatively simple* prognostic model that can be easily tested and is subject to refinement.

Acknowledgments. This work has evolved out of a long association with John Toole, Raymond Schmitt, and the High-Resolution Profiler Group (Ellyn Montgomery, Dave Wellwood, and Gwyneth Packard) at the Woods Hole Oceanographic Institution. Their continuing scientific advice and technical support are greatly appreciated. I am indebted to Alister Adcroft for his assistance with the numerical scheme. An anonymous reviewer is to be thanked for stressing the absence of momentum conservation associated with the eikonal representation. Chris Garrett was adamant in his opinion that the transport scheme not be motivated solely

through the use of (6) and instead suggested the use of dimensional arguments to obtain the scaling for the spatial dimension in (16). Conversations with Yuri Lvov, Estaban Tabak, and Raffaele Ferrari provided the author with much clearer insight into resonant interactions. This manuscript was proofread and edited for journal submission by Anne-Marie Michael. Financial support from the National Science Foundation (Grant OCE 94-15589) and the office of Naval Research (Grant N00014097-1-0087) is gratefully acknowledged.

REFERENCES

Anderson, S. P., 1992: Shear, strain and thermohaline fine structure in the upper ocean. Ph.D. dissertation, University of California, San Diego, 173 pp.

Bell, T. H., 1975: Lee waves in stratified flows with simple harmonic time dependence. *J. Fluid Mech.,* **67,** 705–722.

Bretherton, F. P., and C. Garrett, 1969: Wavetrains in inhomogeneous moving media. *Proc. Roy. Soc. London,* **302A,** 529–554.

Cairns, J. L., and G. O. Williams, 1976: Internal wave observations from a midwater float. *J. Geophys. Res.,* **81,** 1943–1950.

Carnevale, G. F., and J. S. Fredricksen, 1983: A statistical dynamical theory of strongly nonlinear internal waves. *Geophys. Astrophys. Fluid Dyn.,* **23,** 175–207.

Carter, G. S., and M. C. Gregg, 2002: Intense, variable mixing near the head of Monterey Submarine Canyon. *J. Phys. Oceanogr.,* **32,** 3145–3165.

Gargett, A. E., 1990: Do we really know how to scale the turbulent kinetic energy rate ϵ due to breaking of oceanic internal waves? *J. Geophys. Res.,* **95,** 15 971–15 974.

——, P. J. Hendricks, T. B. Sanford, T. R. Osborn, and A. J. Williams III, 1981: A composite spectrum of vertical shear in the ocean. *J. Phys. Oceanogr.,* **11,** 1258–1271.

Garrett, C. J. R., and W. H. Munk, 1972: Space–time scales of internal waves. *Geophys. Fluid. Dyn.,* **2,** 225–264.

——, and ——, 1975: Space–time scales of internal waves. A progress report. *J. Geophys. Res.,* **80,** 291–297.

——, and ——, 1979: Internal waves in the ocean. *Annu. Rev. Fluid Mech.,* **11,** 339–369.

Goff, J. A., 1992: Quantitative characterization of abyssal hill morphology along flow lines in the Atlantic Ocean. *J. Geophys. Res.,* **97,** 9183–9202.

Gregg, M. C., 1987: Diapycnal mixing in the thermocline. A review. *J. Geophys. Res.,* **92,** 5249–5286.

——, 1989: Scaling turbulent dissipation in the thermocline. *J. Geophys. Res.,* **94,** 9686–9698.

——, T. B. Sanford, and D. P. Winkel, 2003: Reduced mixing from the breaking of internal waves in equatorial waters. *Nature,* **422,** 513–515.

Henyey, F. S., 1984: Transport of small-scale internal waves toward microstructure. *Internal Gravity Waves and Small Scale Turbulence: Proc. 'Aha Huliko'a Hawaiian Winter Workshop,* Honolulu, HI, University of Hawaii at Manoa, 201–220.

——, 1991: Scaling of internal wave model predictions for ϵ. *Dynamics of Ocean Internal Gravity Waves: Proc. 'Aha Huliko'a Hawaiian Winter Workshop,* Honolulu HI, University of Hawaii at Manoa, 233–236.

——, J. Wright, and S. M. Flatté, 1986: Energy and action flow through the internal wave field. An eikonal approach. *J. Geophys. Res.,* **91,** 8487–8495.

Kunze, E., A. J. Williams III, and M. G. Briscoe, 1990: Interpreting shear and strain finestructure from a neutrally buoyant float. *J. Geophys. Res.,* **95,** 18 111–18 126.

——, R. W. Schmitt, and J. M. Toole, 1995: The energy balance in a warm-core ring's near-inertial critical layer. *J. Phys. Oceanogr.,* **25,** 942–957.

——, L. K. Rosenfeld, G. S. Carter, and M. C. Gregg, 2002: Internal waves in Monterey Submarine Canyon. *J. Phys. Oceanogr.,* **32,** 1890–1913.

Leaman, K. D., and T. B. Sanford, 1975: Vertical energy propagation of inertial waves: A vector spectral analysis of velocity profiles. *J. Geophys. Res.,* **80,** 1975–1978.

Ledwell, J. R., E. T. Montgomery, K. L. Polzin, L. C. St. Laurent, R. W. Schmitt, and J. M. Toole, 2000: Evidence for enhanced mixing over rough topography in the abyssal ocean. *Nature,* **403,** 179–182.

Lvov, Y. V., and E. G. Tabak, 2001: Hamiltonian formalism and the Garrett and Munk spectrum of internal waves in the ocean. *Phys. Rev. Lett.,* **87,** doi:10.1103/PhysRevLett.87.168501.

McComas, C. H., and F. P. Bretherton, 1977: Resonant interaction of oceanic internal waves. *J. Geophys. Res.,* **82,** 1397–1412.

——, and P. Müller, 1981a: Timescales of resonant interactions among oceanic internal waves. *J. Phys. Oceanogr.,* **11,** 139–147.

——, and ——, 1981b: The dynamic balance of internal waves. *J. Phys. Oceanogr.,* **11,** 970–986.

Müller, P., and D. J. Olbers, 1975: On the dynamics of internal waves in the deep ocean. *J. Geophys. Res.,* **80,** 3848–3860.

——, and N. Xu, 1992: Scattering of oceanic internal gravity waves off random bottom topography. *J. Phys. Oceanogr.,* **22,** 474–488.

——, G. Holloway, F. Henyey, and N. Pomphrey, 1986: Nonlinear interactions among internal gravity waves. *Rev. Geophys.,* **24,** 493–536.

Munk, W., 1981: Internal waves and small-scale processes. *Evolution of Physical Oceanography,* B. A. Warren and C. Wunsch, Eds., The MIT Press, 264–291.

Olbers, D. J., 1976: Nonlinear energy transfer and the energy balance of the internal wavefield in the deep ocean. *J. Fluid Mech.,* **74,** 375–399.

Phillips, O. M., 1960: On the dynamics of unsteady gravity waves of finite amplitude, I. *J. Fluid Mech.,* **9,** 193–217.

——, 1977: *The Dynamics of the Upper Ocean.* 2d ed. Cambridge University Press, 336 pp.

Polzin, K. L., 2004: Idealized solutions for the energy balance of the finescale internal wave field. *J. Phys. Oceanogr.,* **34,** 231–246.

——, J. M. Toole, and R. W. Schmitt, 1995: Finescale parameterizations of turbulent dissipation. *J. Phys. Oceanogr.,* **25,** 306–328.

——, ——, J. R. Ledwell, and R. W. Schmitt, 1997: Spatial variability of turbulent mixing in the abyssal ocean. *Science,* **276,** 93–96.

——, E. Kunze, J. M. Toole, and R. W. Schmitt, 2003: The partition of finescale energy into internal waves and subinertial motions. *J. Phys. Oceanogr.,* **33,** 234–248.

Pomphrey, N., J. D. Meiss, and K. M. Watson, 1980: Description of nonlinear internal wave interactions using Langevin methods. *J. Geophys. Res.,* **85,** 1085–1094.

Sun, H., and E. Kunze, 1999a: Internal wave–wave interactions. Part I: The role of internal wave vertical divergence. *J. Phys. Oceanogr.,* **29,** 2886–2904.

——, and ——, 1999b: Internal wave–wave interactions. Part II: Spectral energy transfer and turbulent production. *J. Phys. Oceanogr.,* **29,** 2904–2919.

Tennekes, H., and J. L. Lumley, 1987: *A First Course in Turbulence.* The MIT Press, 300 pp.

Thorpe, S. A., 1975: The excitation, dissipation, and interaction of internal waves in the deep ocean. *J. Geophys. Res.,* **80,** 328–338.

Weller, R. A., D. L. Rudnick, C. C. Eriksen, K. L. Polzin, N. S. Oakey, J. M. Toole, R. W. Schmitt, and R. T. Pollard, 1991: Forced ocean response during the frontal air–sea interaction experiment (FASINEX). *J. Geophys. Res.,* **96,** 8611–8638.

Wijesekera, H., L. Padman, T. Dillon, M. Levine, C. Paulson, and R. Pinkel, 1993: The application of internal-wave dissipation models to a region of strong mixing. *J. Phys. Oceanogr.,* **23,** 269–286.